Diagn Interv Radiol 2011; 17:181–194

GENERAL RADIOLOGY

REVIEW

Dual-energy CT revisited with multidetector CT: review of principles and clinical applications

Muşturay Karçaaltıncaba, Aykut Aktaş

ABSTRACT

Although dual-energy CT (DECT) was first conceived in the 1970s, it was not widely used for CT indications. Recently, the simultaneous acquisition of volumetric dual-energy data has been introduced using multidetector CT (MDCT) with two X-ray tubes and rapid kVp switching (gemstone spectral imaging). Two major advantages of DECT are material decomposition by acquiring two image series with different kVp and the elimination of misregistration artifacts. Hounsfield unit measurements by DECT are not absolute and can change depending on the kVp used for an acquisition. Typically, a combination of 80/140 kVp is used for DECT, but for some applications, 100/140 kVp is preferred. In this study, we summarized the clinical applications of DECT and included images that were acquired using the dual-source CT and rapid kVp switching. In general, unenhanced images can be avoided by using DECT for body and neurological applications; iodine can be removed from the image, and a virtual, non-contrast (water) image can be obtained. Neuroradiological applications allow for the removal of bone and calcium from the carotid and brain CT angiography. Thorax applications include perfusion imaging in patients with pulmonary thromboemboli and other chest diseases, xenon ventilation-perfusion imaging and solitary nodule characterization. Cardiac applications include dual-energy cardiac perfusion, viability and cardiac iron detection. The removal of calcific plaques from arteries, bone removal and aortic stent graft evaluation may be achieved in the vascular system. Abdominal applications include the detection and characterization of liver and pancreas masses, the diagnosis of steatosis and iron overload, DECT colonoscopy and CT cholangiography. Urinary system applications are urinary calculi characterization (uric acid vs. non-uric acid), renal cyst characterization and mass characterization. Musculoskeletal applications permit the differentiation of gout from pseudogout and a reduction of metal artifacts. Recent introduction of iterative reconstruction techniques can increase the use of DECT techniques; the use of dual energy in patients with a high BMI is limited due to noise and the radiation dose. DECT may be a good alternative to PET-CT. Iodine map images can quantify iodine uptake, and this approach may be more effective than obtaining non-contrast and post-contrast images for the diagnosis of a solid mass. Thus, computer-aided detection may be used more effectively in CT applications. DECT is a promising technique with potential clinical applications.

Key words: • *tomography, spiral computed* • *iodine* • *pulmonary embolism* • *gout*

From the Department of Radiology (M.K. ✉ *musturayk@yahoo.com*), Hacettepe University School of Medicine, Ankara, Turkey; and the Department of Radiology (A.A.), Near East University School of Medicine, Lefkoşa, Turkish Republic of Northern Cyprus.

Received 6 September 2010; accepted 7 September 2010.

Published online 14 October 2010
DOI 10.4261/1305-3825.DIR.3860-10.0

Although dual-energy CT (DECT) was first conceived in 1976, it has not been used widely for clinical indications (1–11). Recently, the simultaneous acquisition of dual-energy data has been introduced using multidetector CT (MDCT) with two X-ray tubes and rapid peak kilovoltage (kVp) switching (gemstone spectral imaging, GSI) (12–16). Two major advantages of DECT are material decomposition by the almost simultaneous acquisition of two image series with different kVp (80 and 140 kVp) and the elimination of misregistration artifacts. In general, noncontrast (unenhanced) images can be avoided by using the dual-energy mode for body and neurological applications; iodine can be removed from the image, and a virtual non-contrast (water) image can be acquired. The major advantage of 80-kVp compared to 140-kVp images is a higher image contrast (Fig. 1). Hounsfield unit measurements on DECT are not absolute and can change depending on the kVp used for the acquisition (at different keV). Typically, a combination of 80/140 kVp is used for DECT, but for some applications, 100/140 kVp is preferred. In this study, we summarized the clinical applications of DECT in the brain, chest and abdomen and in the cardiovascular and musculoskeletal systems (Table 1).

Technique and principles

The basic principle of dual-energy is the acquisition of 2 datasets from the same anatomic location with different kVp (usually 80 and 140 kVp) (1, 2, 17, 18). In the early days of CT, consecutive single-slice acquisitions with different kVp were performed as a dual-energy technique, but this method suffered from breathing and partial volume artifacts (1, 2). At present, an entire body can be scanned within seconds using the DECT technique, and thus, misregistration artifacts due to breathing are eliminated.

Currently, three systems are capable of the nearly simultaneous acquisition of dual-energy data during a single breath hold (12, 14, 15): 64-slice dual-source CT (Definition, Siemens Medical Systems; Erlangen, Germany), 128-slice dual-source CT (Definition Flash, Siemens Medical Systems) and high-definition 64-MDCT (Discovery 750 HD, GE Healthcare; Milwaukee, Wisconsin, USA). In the two systems available from Siemens, the two tubes (tubes A and B) use different kVp (80 and 140 kVp), and in 64-MDCT, the kVp switches from 80 to 140 kVp in less than 0.5 ms. In dual systems, there is concern regarding the susceptibility of the system to cardiac motion due to the time difference (75 or 83 ms) between the tube A and tube B acquisitions of the dual-energy data, but the dual-source CT and 64-MDCT have not been compared to evaluate this issue. The technical specifications of the DECT systems are summarized in Table 2.

The images presented in this article were acquired using a 64-slice dual source CT (Definition, Siemens Medical Systems) and a 64-MDCT (Discovery 750HD, GE Healthcare). The DECT data acquired by both systems can be evaluated with a dedicated workstation using dual-energy software that

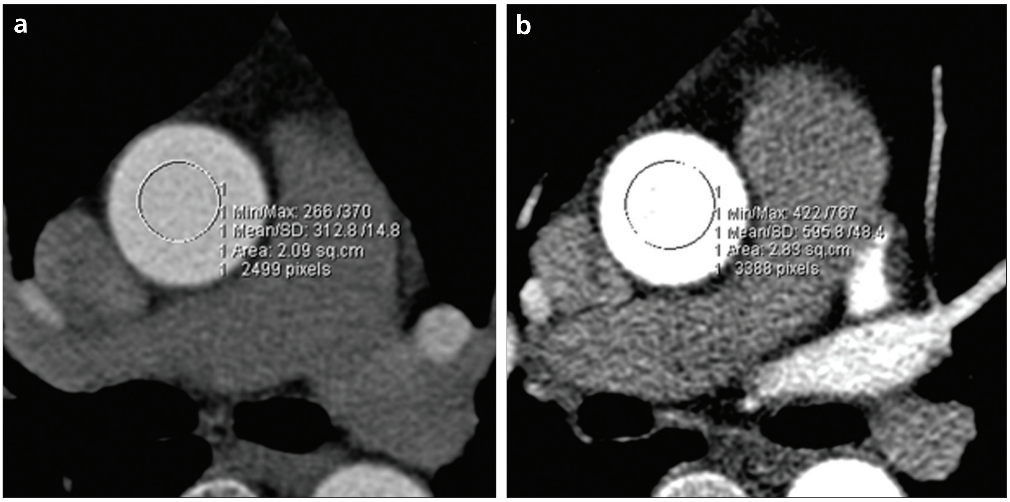

Fig. 1. a, b. Axial DECT images acquired at the level of the pulmonary artery demonstrate the relationship between a Hounsfield unit measurement and kVp. Region of interest (ROI) measurements of the aorta on 140 **(a)** and 80-kVp **(b)** images yielded 312 HU and 595 HU, respectively. The iodine contrast density in the 80-kVp image is almost double that of the 140-kVp image.

Table 1. Potential clinical applications of dual-energy MDCT

Application/technique	Dual-source CT	Fast kVp switching
Neuroradiology		
Calcium removal from carotid arteries	+	+
Virtual non-contrast image for hemorrhage	+	+
Thorax		
Pulmonary perfusion in pulmonary thromboemboli	+	+
Xenon ventilation-perfusion DECT	+	+
Solid nodule characterization	+	+
Cardiac		
Dual-energy cardiac perfusion, viability	+	WIP
Myocardial iron detection	+	+
Vascular		
Removal of calcific plaques	+	+
Bone removal from the image	+	-
Aortic stent graft evaluation	+	+
Gastrointestinal and abdominal		
Virtual non-contrast image for liver, pancreas, any mass	+	+
Liver fat and iron detection	+	+
Gallstone imaging	+	+
Dual-energy CT cholangiography	+	+
Dual-energy CT colonoscopy	+	+
Urinary		
Urinary calculi characterization (uric acid)	+	+
Urinary stone visualization on pyelographic images	+	+
Renal cyst and mass characterization	+	+
Musculoskeletal		
Differential diagnosis of gout and pseudogout	+	+
Metal artifact reduction	-	+
Tendon and ligament visualization	+	+

WIP, work in progress

allows the separation of iodine from the image, and virtual, unenhanced (water) and iodine map images can be obtained easily.

Using dual-source CT, 2 datasets (80 and 140 kVp) are loaded on the workstation, and virtual non-contrast, iodine map, and mixed (with adjustable blending of 80 and 140-kVp data) images can be obtained (Fig. 2) (19, 20). Using 64-MDCT with fast kVp switching, the GSI dataset is loaded on the workstation, and water (virtual non-contrast), iodine, and monochromatic images in addition to spectral data can be obtained using the desired kiloelectron voltage (from 40 to 140 keV) (Fig. 3).

Using dual-source CT, 1-mm rather than 0.625-mm collimation can be used to decrease the noise. Alternatively, a combination of 140/100 kVp rather than 140/80 kVp can be used (21). The second generation dual-source CT (128-slice CT) has a wider field of view (FOV, 33 vs. 26 cm), and a tin filter is used to filter the high-energy spectrum and to increase the image contrast (14, 21, 22). After the addition of a tin filter, it has been proposed that DECT acqui-

Table 2. Technical specifications of dual-energy MDCT systems

Specifications	64-slice dual source MDCT (Definition)	128-slice dual source MDCT (Definition Flash)	64-MDCT (Discovery 750HD)
Detector configuration	2x32x0.625	2x64x0.625	64x0.625
Slice thickness	0.625/1 mm	0.625/1 mm	0.625/1.25 mm
FOV	26 cm	33 cm	50 cm
Time between images	83 ms	75 ms	0.3–0.5 ms
Technique used for dual-energy	2 tubes	2 tubes	Fast kVp switching
Gantry rotation time for dual-energy acquisition	330 ms	300 ms	350 ms
Temporal resolution for dual-energy acquisition	165 ms	150 ms	175 ms

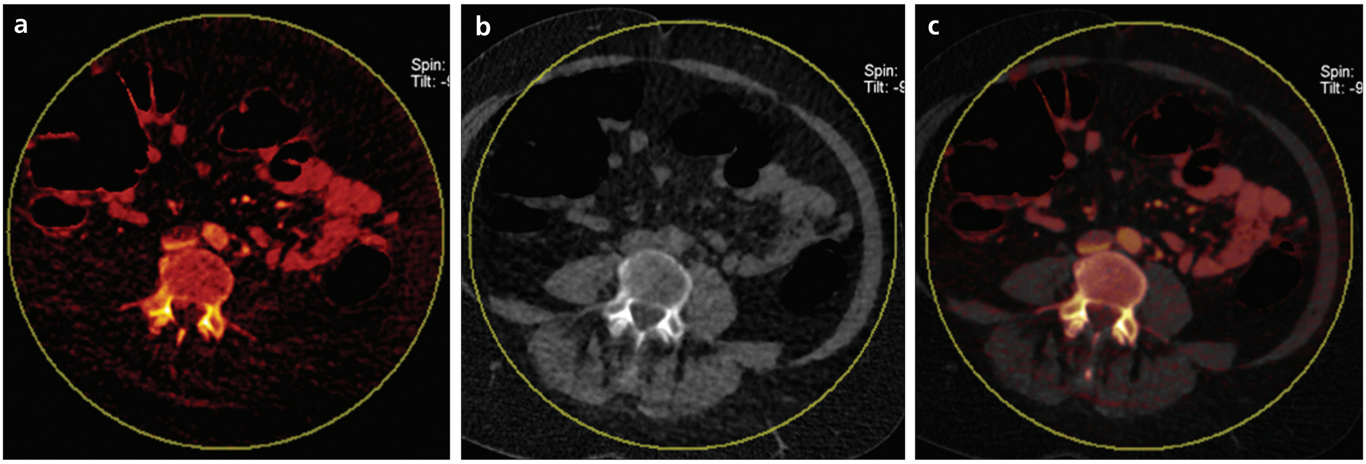

Fig. 2. a–c. Axial DECT images using a dual-source CT. Iodine map **(a)**, virtual non-contrast **(b)** and mixed **(c)** CT images are shown. Note the restriction of the FOV *(yellow circle)* to 26 cm.

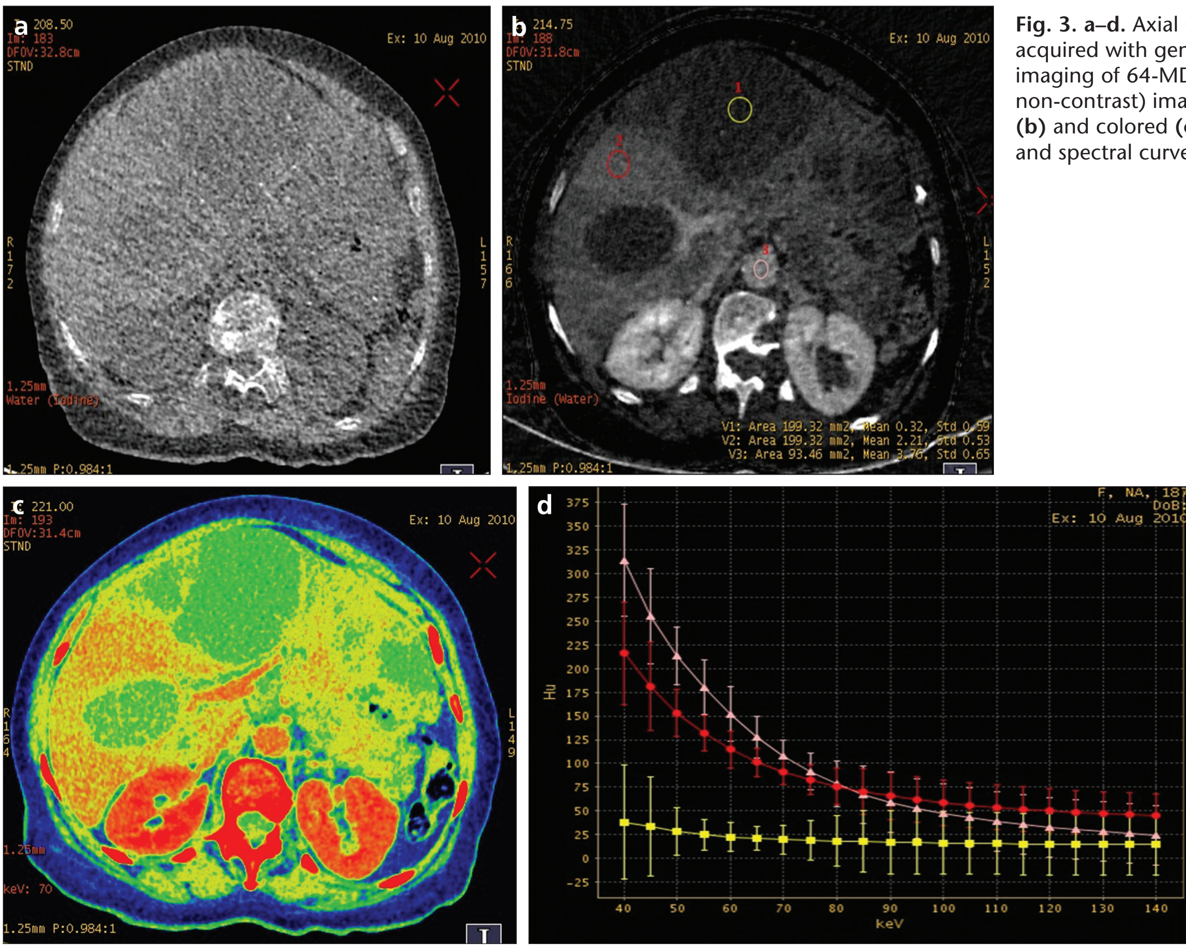

Fig. 3. a–d. Axial CT images acquired with gemstone spectral imaging of 64-MDCT: water (virtual non-contrast) image **(a)**, gray-scale **(b)** and colored **(c)** iodine images and spectral curve **(d)**.

sitions can be obtained concomitantly with single-energy CT (21). Both dual-source CT systems employ z-flying focal spot technology (12, 14).

Potential clinical applications

Neuroradiological applications

Neurological applications permit the generation of virtual non-contrast images for the detection of brain hemorrhages in patients who undergo contrast-enhanced CT angiography (CTA). They also allow the removal of bone and calcium from the carotid and brain CTA (23–36).

It is possible to detect a brain hemorrhage on virtual non-contrast images (Fig. 4), and Gupta et al. (23) have reported sensitivity, specificity and accuracy values of >90% for the detection of a hemorrhage on contrast-enhanced CT images that were acquired from 18 patients using dual-energy. Ferda et al. (24) have used the same technique and reported similar findings in 25 patients, but the contrast-to-noise ratio of the virtual non-contrast images was

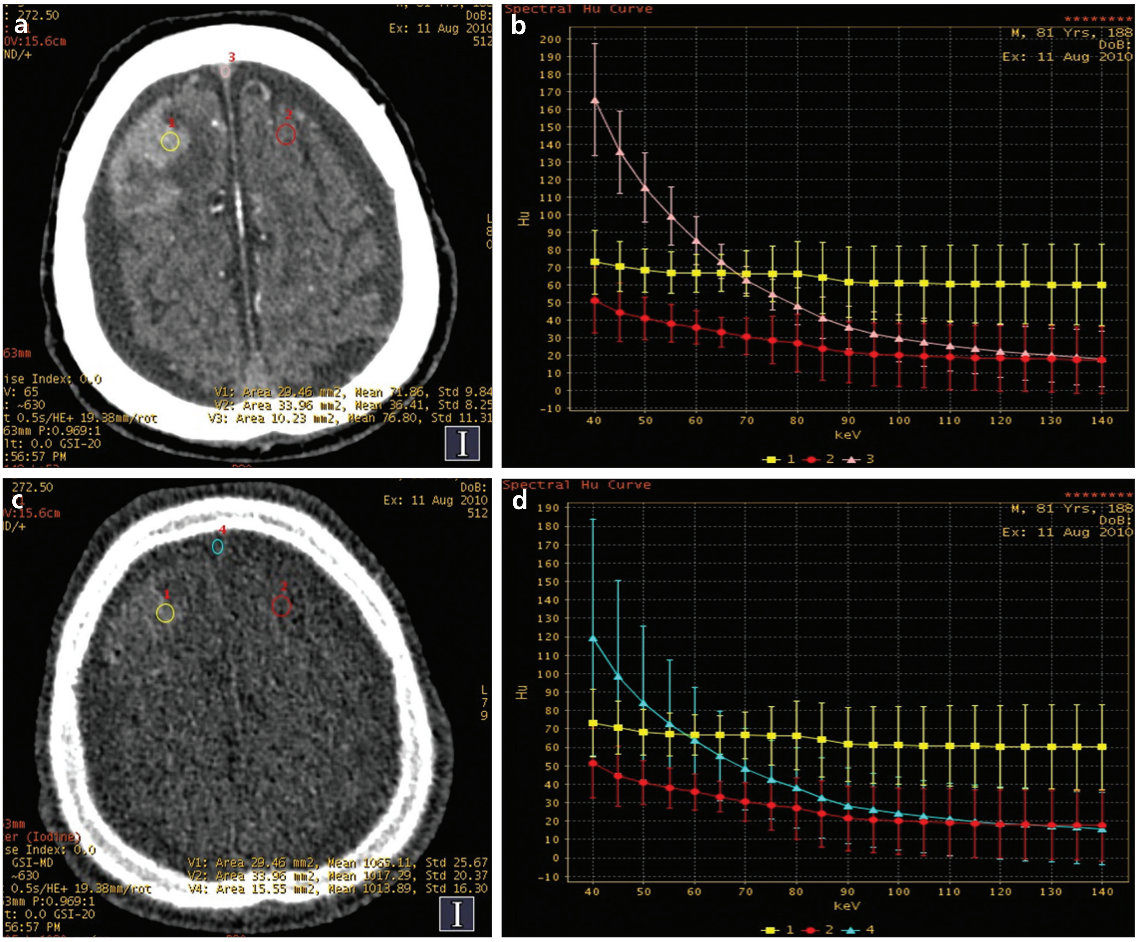

Fig. 4. a–d. Axial images of brain CTA and spectral curve for iodine **(a** and **b)** and water **(c** and **d)** images were acquired using gemstone spectral imaging. Note the hyperdense area on the water (virtual unenhanced) image, which is consistent with hemorrhage. The spectral data show the density of the hemorrhage *(yellow)*, superior sagittal sinus *(white and blue)* and normal area on the iodine **(b)** and water images **(d)** for different keV. No differences in the spectral data for the hemorrhagic area are evident.

lower than that of conventional non-contrast images. In addition, the use of virtual non-contrast images has been reported for the diagnosis of a lipiodol embolism after hepatocellular carcinoma chemoembolization (25).

Several articles have compared dual-energy bone removal to automatic bone removal and digital subtraction CTA, and the dual-energy technique was found to be superior to both techniques, particularly at the level of the skull base (26–35). In addition, the radiation dose was reduced as compared to digital subtraction CTA (26, 27, 31). The removal of calcium from the carotid artery using dual-energy methods may lead to an overestimation of the degree of stenosis when compared to DSA (29). Newer dual-source MDCTs with a 33-cm FOV that generate 100 and 140 kVp images may provide better vessel integrity and image quality at the level of the shoulder (33).

Thorax applications

The major advantages of DECT in thoracic applications are a lack of misregistration and visualization of the lung perfusion and ventilation (37–59). Misregistration is avoided due to the simultaneous acquisition of 80 and 140 kVp images. In patients with pulmonary thromboembolism, DECT may allow the detection of subtle emboli by revealing perfusion defects (Fig. 5). Several articles have assessed the role of DECT in the diagnosis of pulmonary thromboembolism (37–44). Krisska et al. (40) obtained a high negative predictive value by using perfusion images. Chae et al. (41) proposed a perfusion defect score that demonstrated a good correlation to the right ventricle/left ventricle diameter ratio and the CTA obstruction score. In addition, an assessment of the lung perfusion can allow the visualization of pathologies that have been previously unknown, particularly in patients with interstitial lung disease, emphysema, asthma, or chronic thromboembolic disease and in patients with tumors (45–50). Recently, the introduction of Xenon DECT enabled the collection of ventilation-perfusion CT acquisitions, and in the future, it may replace ventilation-perfusion scintigraphy (51–54). Ferda et al. (55) have reported the use of perfusion and minimum intensity projection (minIP) images for the assessment of iodine and air distributions. The superior registration of DECT may demonstrate the presence or lack of enhancement of sub-centimeter and solitary lung nodules (Fig. 6) (56, 57). Schenzle et al. (21) have reported that dual-energy methods for the thorax are feasible without the additional radiation dose provided by dual-source CT. A change of the collimation from 0.6 to 1.2 mm is required to achieve dose neutrality for the 140/80-kVp combi-

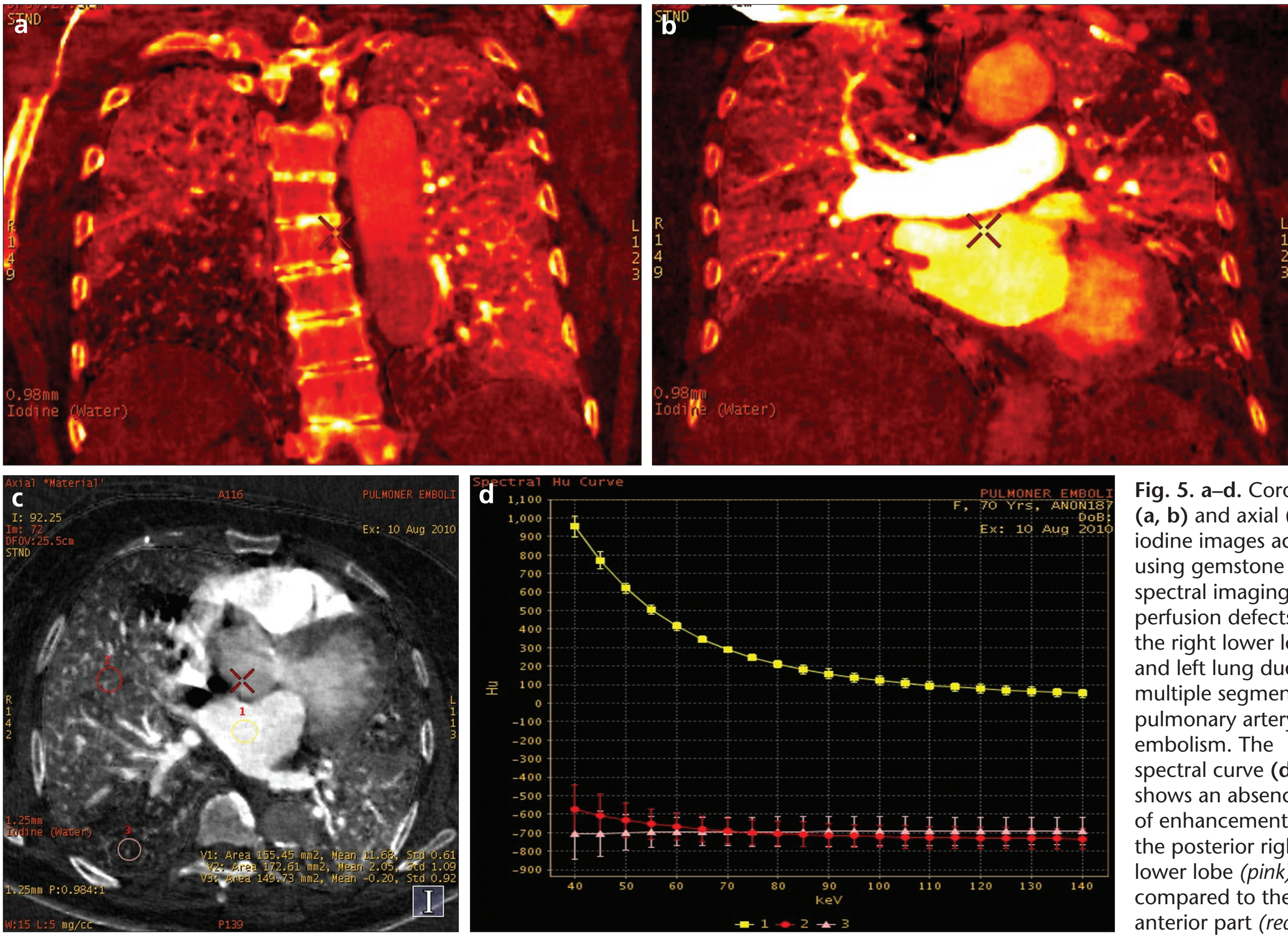

Fig. 5. a–d. Coronal **(a, b)** and axial **(c)** iodine images acquired using gemstone spectral imaging show perfusion defects in the right lower lobe and left lung due to multiple segmental pulmonary artery embolism. The spectral curve **(d)** shows an absence of enhancement in the posterior right lower lobe *(pink)* as compared to the anterior part *(red)*.

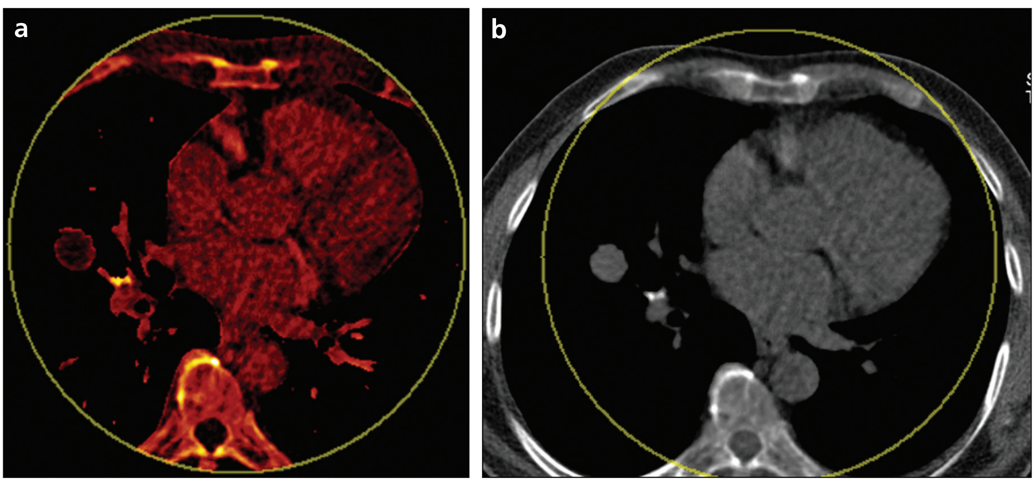

Fig. 6. a, b. Axial iodine map **(a)** and virtual non-contrast **(b)** images acquired using dual-source CT show an absence of enhancement and calcification within the solitary lung nodule on the right side.

nation without a tin filter; however, this procedure is not needed for the 140/100-kVp combination with a tin filter (19).

Cardiac applications

Clinical applications of cardiac DECT have been described for dual-energy perfusion with or without the adenosine stress test, viability imaging and cardiac iron detection (6, 58–67) (Fig. 7). To decrease the image noise for cardiac applications, 100 and 140-kVp acquisitions are preferred (59, 60). The addition of an iterative reconstruction technique may allow a better image quality for cardiac applications. Ruzsics et al. (61) were the first to describe the combination of dual-energy cardiac perfusion and coronary CTA. The authors used this technique to diagnose coronary artery stenosis and myocardial ischemia. In addition, DECT together with an adenosine stress test has been recently described (62, 63). The acquisition of dual-energy cardiac perfusion combined with coronary CT images can be difficult in patients with elevated heart rates due to a worsening of the temporal resolution from 83 to 165 ms in the dual-source CT (64). Therefore, dual-energy technique is preferred in patients with low heart rates (<65 bpm).

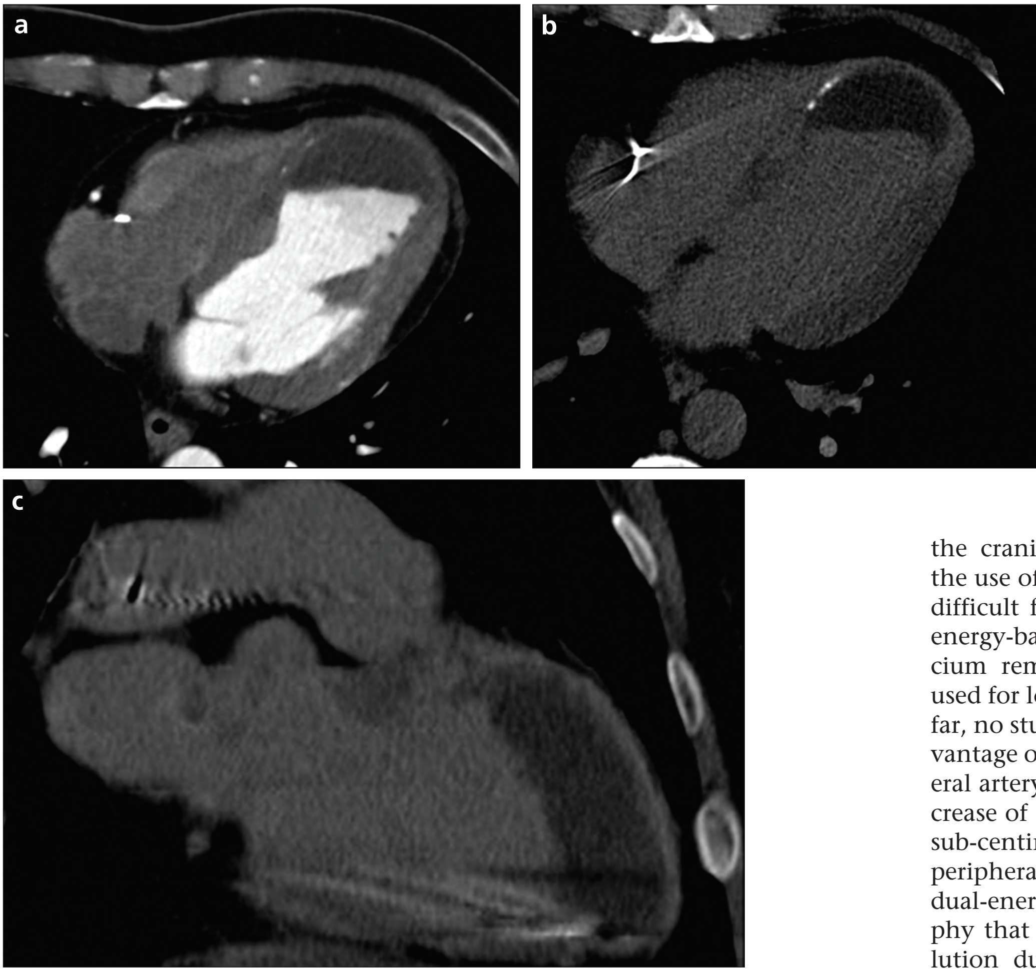

Fig. 7. a–c. Arterial-phase 4-chamber **(a)**, delayed-enhanced 4-chamber **(b)** and 2-chamber **(c)** 80-kVp DECT images were acquired by dual-source CT. Note the superior distinction of the apical thrombus from the viable myocardium on the delayed DECT images.

The detection of acute myocardial infarction has been investigated in a canine model using DECT, and a sensitivity and specificity of 92% and 80%, respectively, were obtained by comparing the iodine map images with the results obtained via a histopathological analysis (66). Bauer et al. (65) have used late enhancement DECT to identify chronic myocardial infarction areas and viability and compared the results to those obtained using 3T MRI. They reported a sensitivity of 77%, a specificity of 97%, a positive predictive value of 85%, a negative predictive value of 96% and an accuracy of 94% for the detection of myocardial scarring (65).

Several articles have assessed the role of DECT for the characterization of plaques, for calcific plaque removal from coronary arteries and for the evaluation of coronary stents in *in vitro* and *ex vivo* settings (68–72). Tanami et al. (68) have reported that lower energy settings with a dual-energy method demonstrate a superior diagnostic performance for plaque characterization in an ex vivo setting.

Cardiac iron can be detected by DECT, and therefore, this technique could be useful for patients who cannot undergo cardiac MRI due to claustrophobia or other contraindications (Fig. 8) (67).

Vascular applications

Aortic stent grafting is being used increasingly for aortic aneurysms, and the imaging protocol consists of unenhanced, arterial and venous phase images. This protocol exposes the patient to a high radiation burden because it is repeated every six months. The dual-energy aortic stent graft protocol may obviate the need for unenhanced CT, and iodine map images may facilitate the recognition of endoleaks (73–77).

The precise removal of calcium from arteries can facilitate a better evaluation of atherosclerotic arteries (78). A dual-energy data acquisition can permit the faster removal of calcific plaques in large arteries and bony structures in the cranial region (Fig. 9). However, the use of this technique appears to be difficult for small-sized arteries. Dual-energy-based bone removal and calcium removal techniques have been used for lower extremity CTA, but thus far, no study has demonstrated any advantage of dual-energy CTA for peripheral artery applications (79–84). An increase of the radiation dose, noise and sub-centimeter diameter of the distal peripheral arteries are limitations for dual-energy peripheral CT angiography that may be solved by high-resolution dual-energy acquisitions combined with iterative reconstruction and spectral filtering. DECT has been reported to improve the in vitro differentiation between soft tissues that are present in plaques; however, further studies are needed for confirmation of these results (85).

Gastrointestinal and abdominal applications

The use of dual-energy has revealed that 80-kVp images demonstrate a better image contrast than do 140-kVp images (15, 20, 86–88). This phenomenon appears to be useful for the evaluation of enhanced liver lesions in the arterial phase in hepatocellular carcinoma and in hypervascular liver metastases. Marin et al. (15) compared 80 and 140-kVp images to detect hypervascular lesions in vitro and in vivo, and they found that 80-kVp images with a high mA enabled the visualization of a greater number of lesions compared to 140-kVp images. Robinson et al. (89) found that 80-kVp images were superior for of the distinction of metastases and normal liver tissue. However, there is a role for iterative reconstruc-

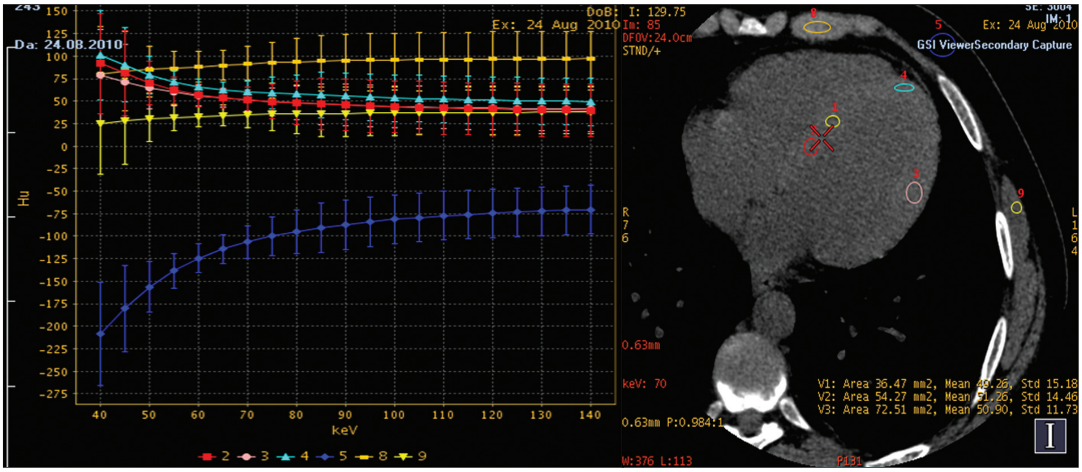

Fig. 8 Axial DECT image from the left ventricle acquired by gemstone spectral imaging without the administration of contrast shows a hyperdense appearance of the left ventricle myocardium. Spectral analysis of the myocardium *(red, pink and blue circles),* intercostal muscles *(yellow)* and subcutaneous fat shows an increased density of the myocardium in the lower keV spectrum compared to the spectral pattern observed for subcutaneous fat and intercostal muscles.

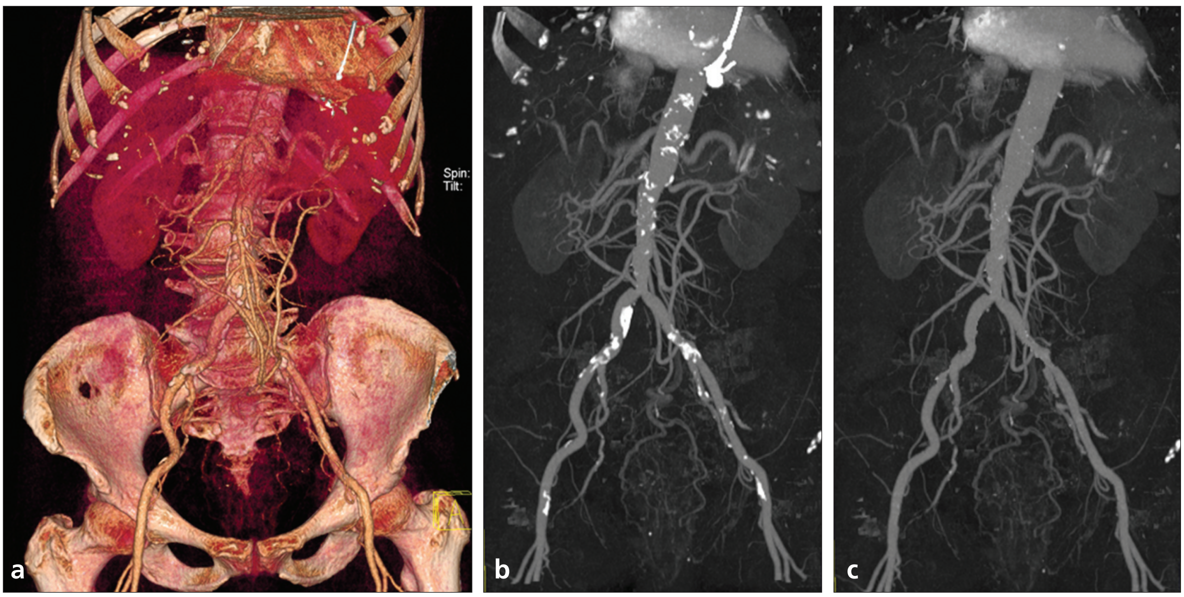

Fig. 9. a–c. Coronal volume-rendered **(a)** MIP, **(b** and **c)** DECT angiography images acquired by dual-source CT show dual-energy bone removal **(b)** and calcific plaque removal **(c)**.

tion techniques in clinical applications to decrease the image noise of 80-kVp images (90). Kim et al. (91) used a different weighting factor for blended or mixed images, and they found that linear blending methods with a low level and a high width were the most useful for the detection of hepatocellular carcinoma.

The elimination of unenhanced CT images can be an advantage of DECT. Zhang et al. (92) recently reported that the avoidance of non-contrast CT in a multiphasic CT protocol might reduce the radiation dose. De Cecco et al. (93) reported similar findings, but they stated that an optimal virtual non-contrast image was only possible in patients with a low BMI.

DECT has been used for the diagnosis of liver iron and fat, which display opposite spectral patterns (6, 86, 94). The measured density of a liver increases with decreasing kVp and KeV in patients with hepatic iron overload, but the measured density of a liver decreases with decreasing kVp and KeV in patients with steatosis (Fig. 10).

Dual-energy cholangiography has been described, and it may facilitate the detection of bile ducts and the measurement of biliary segment dimensions (86, 95). In vitro studies have been performed to characterize the dual-energy of gallstones, and a similar protocol may be used for patients with biliary dilatation and a suspected choleduct stone (86, 96, 97).

The use of 80-kVp data obtained by DECT may permit a better distinction of pancreatic adenocarcinoma from the adjacent normal parenchyma by increasing the conspicuity of the masses (98, 99).

DECT colonoscopy

Karcaaltincaba et al. (100) were the first group to describe a DECT colonoscopy technique that has the potential to obviate non-contrast prone images from diagnostic CT colonoscopy protocols. Colonic polyps and masses are enhanced approximately 40–50 HU on post-contrast images. Thus, the enhancement of colonic masses can be differentiated from stool through the use of iodine DECT images, and non-

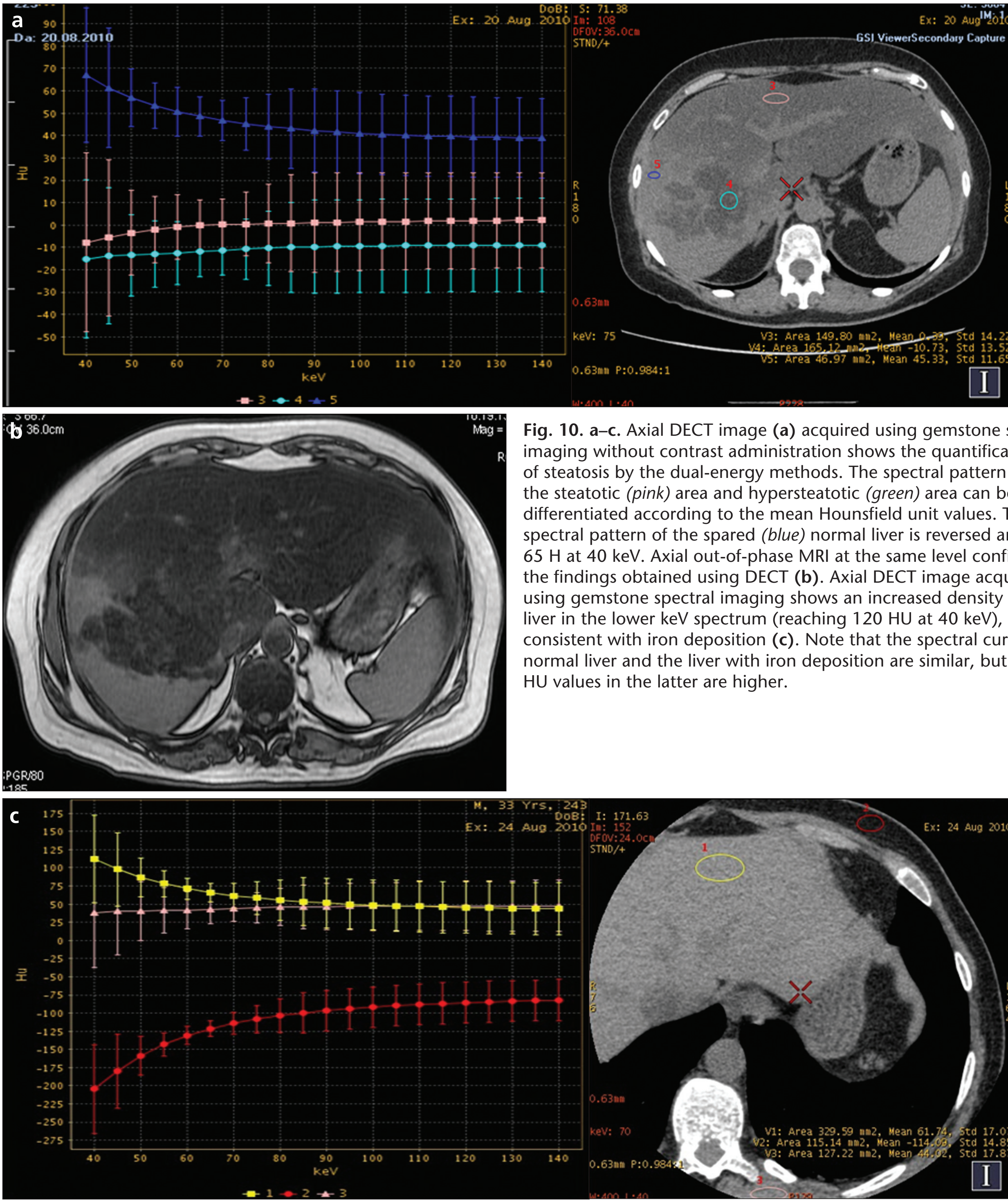

Fig. 10. a–c. Axial DECT image **(a)** acquired using gemstone spectral imaging without contrast administration shows the quantification of steatosis by the dual-energy methods. The spectral pattern of the steatotic *(pink)* area and hypersteatotic *(green)* area can be differentiated according to the mean Hounsfield unit values. The spectral pattern of the spared *(blue)* normal liver is reversed and reaches 65 H at 40 keV. Axial out-of-phase MRI at the same level confirms the findings obtained using DECT **(b)**. Axial DECT image acquired using gemstone spectral imaging shows an increased density of the liver in the lower keV spectrum (reaching 120 HU at 40 keV), which is consistent with iron deposition **(c)**. Note that the spectral curves for the normal liver and the liver with iron deposition are similar, but the mean HU values in the latter are higher.

cathartic DECT colonoscopy may be feasible, especially in elderly patients (Fig. 11). DECT may also be used for spectral electronic cleansing in reduced catharsis CT colonoscopy (101).

Urinary applications

Urinary system applications include the diagnosis of uric acid and cystine stones, the detection of urinary stones in contrast-enhanced CT studies and the characterization of renal masses and cysts (Fig. 12) (102–117).

Dual-energy data can be used to characterize urinary stones. Using in vitro and in vivo settings, several articles on this topic have yielded promising results regarding the differentiation of uric acid stones from calcium stones (102–111). However, a major disadvantage of this technique is an increased dose of radiation in comparison to the standard protocol. We believe that the use of this technique is justified only for the characterization of urinary stones. Therefore, the standard protocol should be used to detect stones, and if necessary, limited scanning at the stone location in dual-energy mode can facilitate the characterization of a stone without

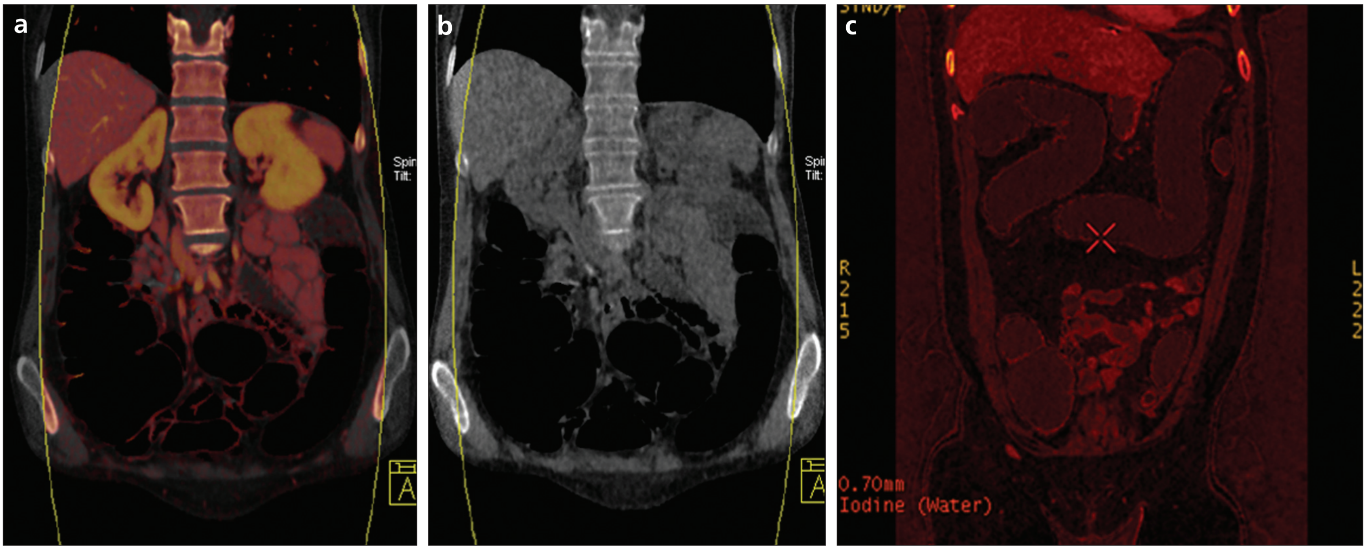

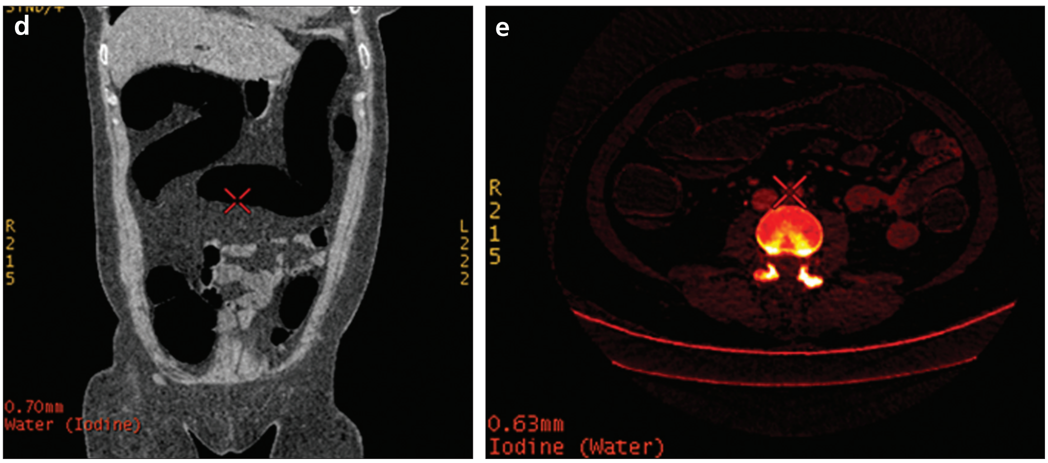

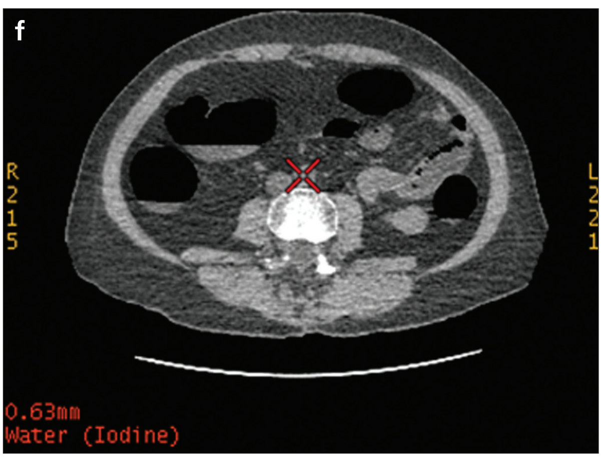

Fig. 11. a–f. DECT colonoscopy iodine **(a, c, e)** and virtual non-contrast **(b, d, f)** images acquired by dual-source CT **(a, b)** and gemstone spectral imaging **(c–f)** show the absence of a polipoid lesion. Note the lack of FOV restriction on the images obtained by fast kVp switching **(c–f)**. The iodine DECT colonoscopy image **(e)** shows an absence of fluid enhancement in the right colon segments.

a significant radiation burden to the patient. The addition of a spectral filter to the dual-source CT did not improve the subgroup characterization of calcium-containing stones (110, 111). Furthermore, dual-energy techniques have been used for the diagnosis of renal stones on CT pyelography images through the use of virtual non-contrast images; however, this technique is limited for the diagnosis of small (<2 mm) renal stones (112, 113).

Graser et al. (114, 115) have published two studies using first and second-generation dual-source CTs to assess the role of renal mass characterization with the dual-energy method. In these studies, the omission of a non-contrast CT could result in a 35% (first generation) and a 50% (second generation) reduction of the radiation dose. In the latter study, they reported an accuracy of 95% for the single-phase DECT protocol in comparison to a correlative accuracy value of 96% for the dual-phase renal mass CT protocol (115). Similar findings have been reported by Leschka et al. and Brown et al. (116, 117) in phantom models. Recently, the possibility of differentiating renal proxies that contain protein, blood and iodine has been reported (118).

Adrenal gland applications

Gupta et al. (119) have reported the application of DECT to characterize adrenal nodules (Fig. 12). A decrease in attenuation at 80 kVp resulted in a diagnosis of adrenal adenoma with a sensitivity of 50%, a specificity of 100%, a positive predictive value of 100% and a negative predictive value of 28%.

Musculoskeletal applications

The most useful musculoskeletal system application of dual-energy

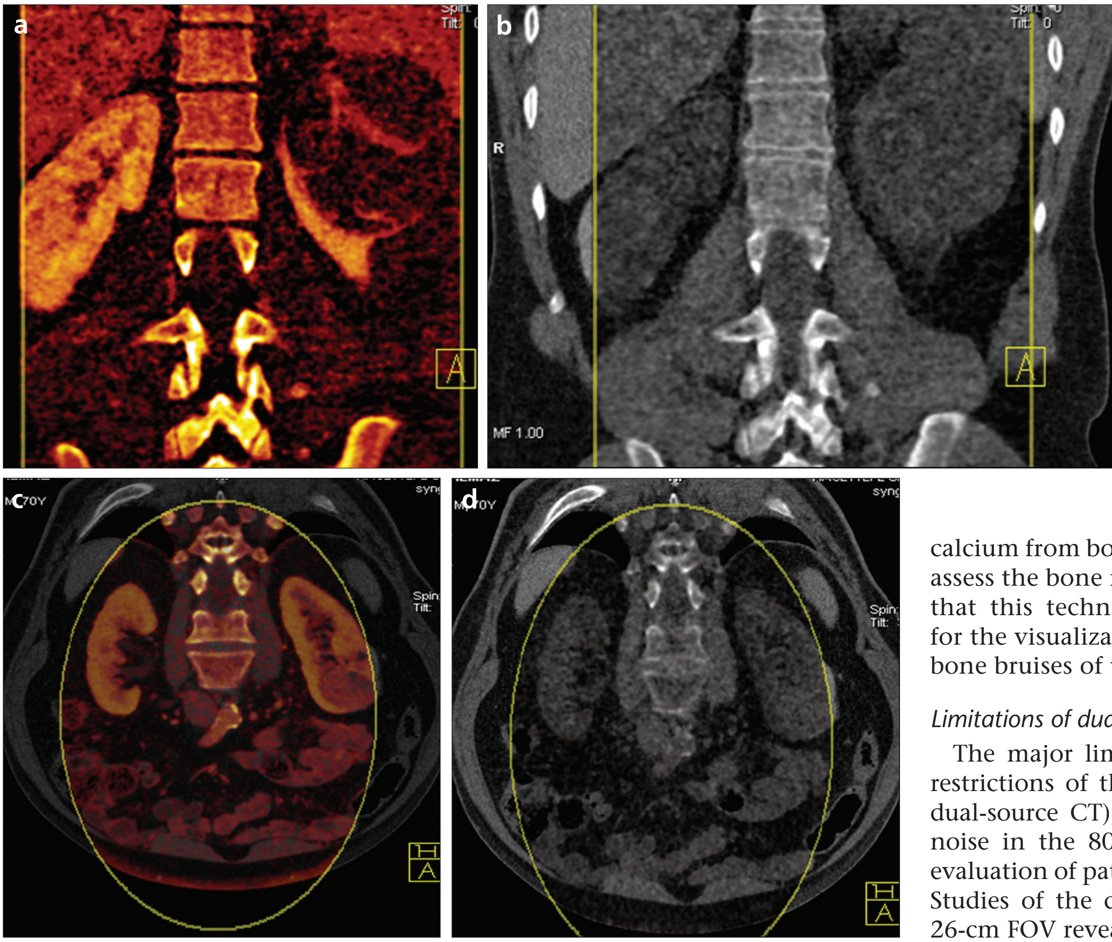

Fig. 12. a–d. Coronal DECT images obtained by dual-source CT. A contrast enhancement in the septa of the left renal cystic lesion is evident on the iodine map **(a)**. Note the absence of calcification on the virtual non-contrast image **(b)**. An enhancement of the solid renal mass in the left lower pole is clearer on the iodine map **(c)** in comparison to the virtual non-contrast image **(d)**.

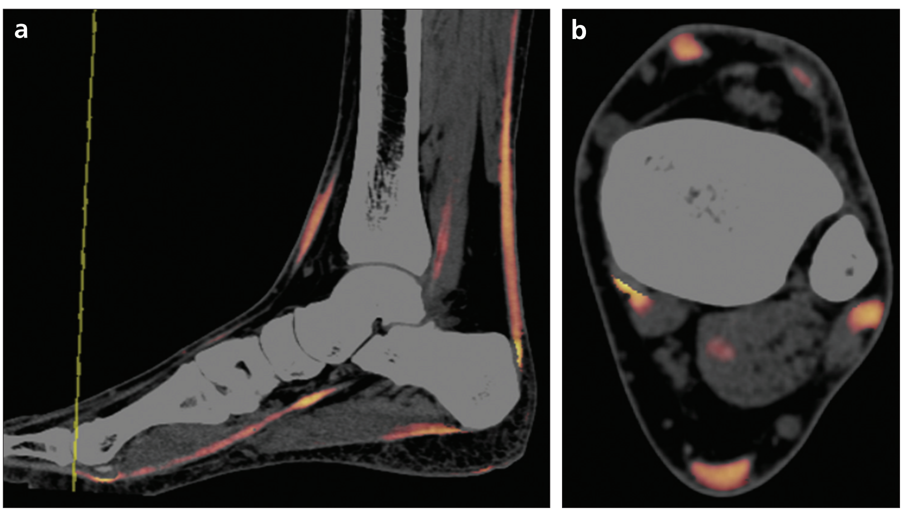

Fig. 13. a, b. Sagittal **(a)** and axial **(b)** DECT images of an ankle that were obtained using dual-source CT without contrast administration. The images show the color coding of extensor and flexor tendons.

is the differentiation of gout and pseuodgout via the diagnosis of uric acid and calcium crystals in the joint space (120–122). Tendon and ligament visualization has been proposed by CT vendors, but few studies have evaluated this application (Fig. 13) (123–125). CT artrography using the dual-energy technique has also been described (126). Metal artifact reduction has been proposed for the fast kVp switching technique, which employs images with a low keV. Pache et al. (127) have used DECT to subtract calcium from bone. They attempted to assess the bone marrow and suggested that this technique might be useful for the visualization of post-traumatic bone bruises of the knee.

Limitations of dual-energy MDCT

The major limitations of DECT are restrictions of the field of view (with dual-source CT), high radiation dose, noise in the 80-kVp images and the evaluation of patients with a high BMI. Studies of the dual-source CT with a 26-cm FOV revealed a higher radiation dose in comparison to single-energy acquisitions (<30%) (100, 128). The addition of a tin filter has been suggested to decrease the radiation dose, and Schenzle et al. (21) have reported that the application of DECT with a tin filter can be performed without an additional dose of radiation, as compared to single-energy acquisitions. However, these findings must be confirmed in future studies. Ho et al. (16) have measured the radiation dose of dual-energy (with fast kVp switching) and single-energy MDCT using abdominal imaging protocols. The effective dose ranges from 22.5 to 36.4 mSv and from 9.4 to 13.8 mSv for DECT and single-energy CT imaging, respectively. An increased radiation dose can be justified when unenhanced CT images are eliminated from the CT protocols, which may result in an overall radiation dose saving (92, 93, 105, 106). Beam-hardening artifacts can be observed in thorax perfusion DECT due to the dense contrast in the superior vena cava, which can mimic an embolus. These artifacts can be minimized by the use of saline flushing and caudo-cranial scanning (129).

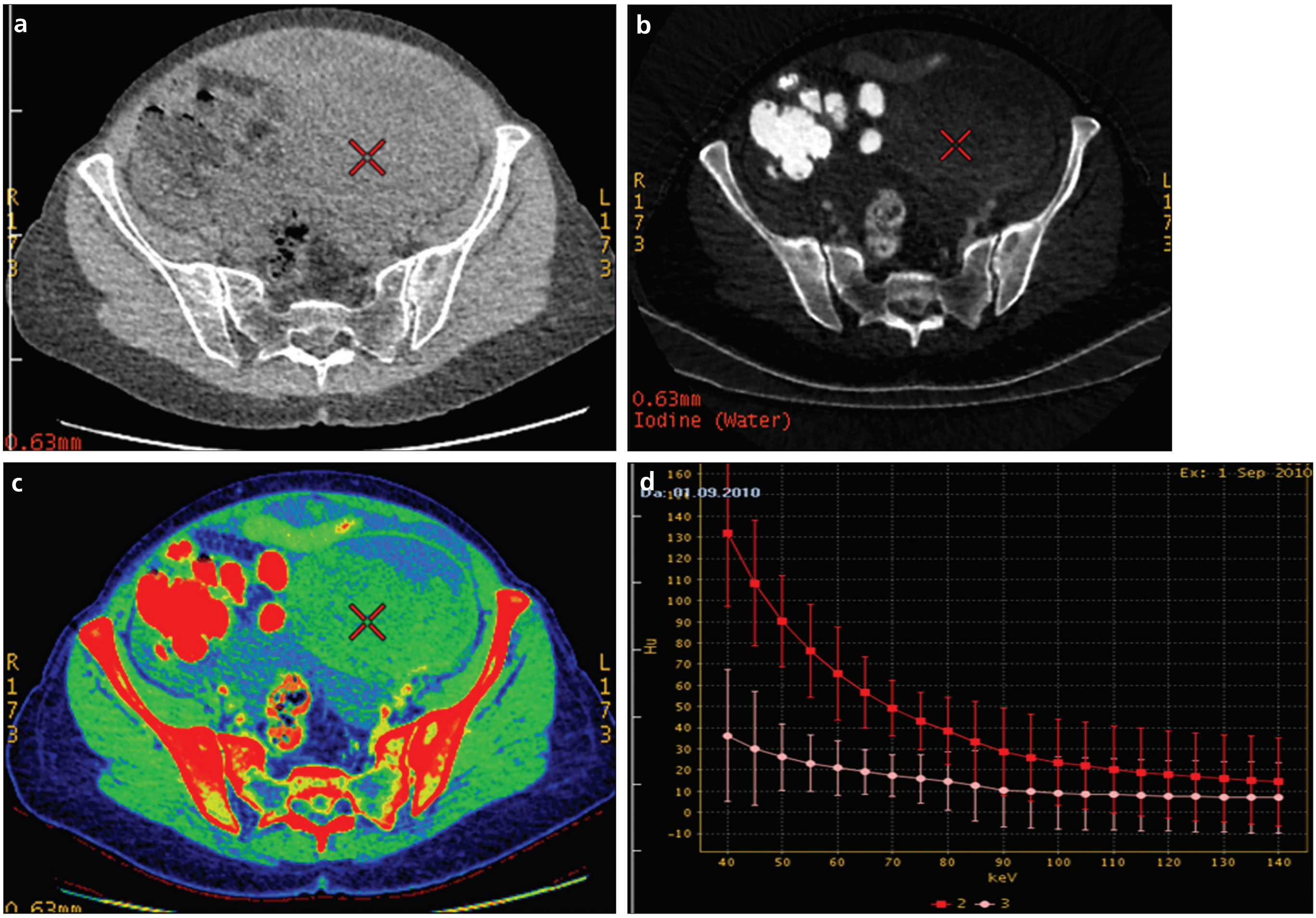

Fig. 14. a–d. Axial water **(a)**, gray-scale iodine **(b)** and colored iodine **(c)** (70 keV) DECT images obtained by fast kVp switching show a left ovarian mass. Spectral curves **(d)** for the solid *(red)* and cystic *(pink)* parts of the ovarian tumor are evident.

Future prospects

DECT as an alternative to PET-CT

Although PET-CT is a commonly used technique, in particular for tumor staging, a variety of difficulties limits the usefulness of this technique. Misregistration is a significant issue in PET-CT. The duration of the PET portion of a PET-CT study is longer (30–40 min) than that of the CT portion (<1 min). Therefore, PET images are acquired during free breathing, and CT images are acquired within a single breath hold. Misregistration limits the usefulness of PET-CT for the detection of small lesions, particularly in the lungs. In contrast, DECT enables perfect registration due to the almost simultaneous acquisition of 80- and 140-kVp data, which are not affected by breathing and movement artifacts. PET-CT is an excellent tool for the demonstration of glucose metabolism, which is extremely useful in oncologic imaging. However, post-operative changes, post-radiation changes, granulomatous reactions, intense inflammation and infection can cause glucose hypermetabolism, which may mimic a tumor on PET-CT images. Angiogenesis is another important feature of cancer cells that can be demonstrated by MR or CT perfusion. DECT imaging provides iodine maps that have the potential to allow an objective determination of contrast enhancement or iodine uptake independently of the anatomic background (Fig. 14). This feature may facilitate an increased detection of lesions due to better contrast detection, which can be displayed on maximum intensity projection (MIP) and color-coded images in a manner similar to PET-CT images. In addition, iodine maps may be used for the objective assessment of disease activity, especially in patients who have undergone a targeted antitumor treatment.

Conclusion

Volumetric DECT acquisition enables the emergence of new applications with potential benefits. The major advantages of DECT are material decomposition, the separation of iodine from the image and the prevention of misregistration, particularly in the thorax and abdomen. However, in patients with a high BMI, noise constraints may result in a suboptimal image quality. The use of iterative reconstruction techniques can facilitate the wider use of DECT applications by decreasing the noise and the radiation dose. These technologies may eventually lead to the better detection and characterization of lesions in the body and an objective evaluation of iodine uptake by various organs (e.g., heart, lung, liver, kidney, intestine). Computer-aided detection algorithms can be developed for this purpose.

Conflict of interest disclosure

The authors declared no conflicts of interest.

References

1. Rutherford RA, Pullan BR, Isherwood I. X-ray energies for effective atomic number determination. Neuroradiology 1976; 11:23–28.
2. Alvarez RE, Macovski A. Energy-selective reconstructions in x-ray computerized tomography. Phys Med Biol 1976; 21:733–744.
3. Marshall W, Hall E, Doost-Hoseini A, Alvarez R, Macovski A, Cassel D. An implementation of dual energy CT scanning. J Comput Assist Tomogr 1984; 8:745–749.
4. Dunscombe PB, Katz DE, Stacey AJ. Some practical aspects of dual-energy CT scanning. Br J Radiol 1984; 57:82–87.
5. Cann CE, Gamsu G, Birnberg FA, Webb WR. Quantification of calcium in solitary pulmonary nodules using single- and dual-energy CT. Radiology 1982; 145:493–496.
6. Goldberg HI, Cann CE, Moss AA, Ohto M, Brito A, Federle M. Noninvasive quantitation of liver iron in dogs with hemochromatosis using dual-energy CT scanning. Invest Radiol 1982; 17:375–380.
7. Chiro GD, Brooks RA, Kessler RM, et al. Tissue signatures with dual-energy computed tomography. Radiology 1979; 131:521–523.
8. Kelcz F, Joseph PM, Hilal SK. Noise considerations in dual energy CT scanning. Med Phys 1979; 6:418–425.
9. Montner SM, Lehr JL, Oravez WT. Quantitative evaluation of a dual energy CT system. J Comput Assist Tomogr 1987; 11:144–150.
10. Hawkes DJ, Jackson DF, Parker RP. Tissue analysis by dual-energy computed tomography. Br J Radiol 1986; 59:537–542.
11. Hemmingsson A, Jung B, Ytterbergh C. Dual energy computed tomography: simulated monoenergetic and material-selective imaging. J Comput Assist Tomogr 1986; 10:490–499.
12. Flohr TG, McCollough CH, Bruder H, et al. First performance evaluation of a dual-source CT (DSCT) system. Eur Radiol 2006; 16:256–268.
13. Johnson TR, Krauss B, Sedlmair M, et al. Material differentiation by dual energy CT: initial experience. Eur Radiol 2007; 17:1510–1517.
14. Petersilka M, Bruder H, Krauss B, Stierstorfer K, Flohr TG. Technical principles of dual source CT. Eur J Radiol 2008; 68:362–368.
15. Marin D, Nelson RC, Samei E, et al. Hypervascular liver tumors: low tube voltage, high tube current multidetector CT during late hepatic arterial phase for detection--initial clinical experience. Radiology 2009; 251:771–779.
16. Ho LM, Yoshizumi TT, Hurwitz LM, Nelson RC, Marin D, Toncheva G, Schindera ST. Dual energy versus single energy MDCT: measurement of radiation dose using adult abdominal imaging protocols. Acad Radiol 2009; 16:1400–1407.
17. Wang G, Yu H, De Man B. An outlook on x-ray CT research and development. Med Phys 2008; 35:1051–1064.
18. Liu X, Yu L, Primak AN, McCollough CH. Quantitative imaging of element composition and mass fraction using dual-energy CT: three-material decomposition. Med Phys 2009; 36:1602–1609.
19. Yu L, Primak AN, Liu X, McCollough CH. Image quality optimization and evaluation of linearly mixed images in dual-source, dual-energy CT. Med Phys 2009; 36:1019–1024.
20. Fletcher JG, Takahashi N, Hartman R, et al. Dual-energy and dual-source CT: is there a role in the abdomen and pelvis? Radiol Clin North Am 2009; 47:41–57.
21. Schenzle JC, Sommer WH, Neumaier K, et al. Dual energy CT of the chest: how about the dose? Invest Radiol 2010; 45:347–353.
22. Primak AN, Ramirez Giraldo JC, Liu X, Yu L, McCollough CH. Improved dual-energy material discrimination for dual-source CT by means of additional spectral filtration. Med Phys 2009; 36:1359–1369.
23. Gupta R, Phan CM, Leidecker C, et al. Evaluation of dual-energy CT for differentiating intracerebral hemorrhage from iodinated contrast material staining. Radiology 2010; 257:205–211.
24. Ferda J, Novák M, Mírka H, et al. The assessment of intracranial bleeding with virtual unenhanced imaging by means of dual-energy CT angiography. Eur Radiol 2009; 19:2518–2522.
25. Lee CS, Kim SJ, Choi JW, Choi CG, Lee DH. Cerebral lipiodol embolism proven by dual-energy computed tomography: a case report. J Comput Assist Tomogr 2010; 34:105–106.
26. Ma R, Liu C, Deng K, Song SJ, Wang DP, Huang L. Cerebral artery evaluation of dual energy CT angiography with dual source CT. Chin Med J (Engl) 2010; 123:1139–1144.
27. Zhang LJ, Wu SY, Niu JB, et al. Dual-energy CT angiography in the evaluation of intracranial aneurysms: image quality, radiation dose, and comparison with 3D rotational digital subtraction angiography. AJR Am J Roentgenol 2010; 194:23–30.
28. Thomas C, Korn A, Krauss B, et al. Automatic bone and plaque removal using dual energy CT for head and neck angiography: feasibility and initial performance evaluation. Eur J Radiol 2010; 76:61–67.
29. Thomas C, Korn A, Ketelsen D, et al. Automatic lumen segmentation in calcified plaques: dual-energy CT versus standard reconstructions in comparison with digital subtraction angiography. AJR Am J Roentgenol 2010; 194:1590–1595.
30. Lell MM, Kramer M, Klotz E, Villablanca P, Ruehm SG. Carotid computed tomography angiography with automated bone suppression: a comparative study between dual energy and bone subtraction techniques. Invest Radiol 2009; 44:322–328.
31. Deng K, Liu C, Ma R, et al. Clinical evaluation of dual-energy bone removal in CT angiography of the head and neck: comparison with conventional bone-subtraction CT angiography. Clin Radiol 2009; 64:534–541.
32. Uotani K, Watanabe Y, Higashi M, et al. Dual-energy CT head bone and hard plaque removal for quantification of calcified carotid stenosis: utility and comparison with digital subtraction angiography. Eur Radiol 2009; 19:2060–2065.
33. Lell MM, Hinkman F, Nkenke E, et al. Dual energy CTA of the supraaortic arteries: technical improvements with a novel dual source CT system. Eur J Radiol 2010; 76:e6–12.
34. Watanabe Y, Uotani K, Nakazawa T, et al. Dual-energy direct bone removal CT angiography for evaluation of intracranial aneurysm or stenosis: comparison with conventional digital subtraction angiography. Eur Radiol 2009; 19:1019–1024.
35. Morhard D, Fink C, Graser A, Reiser MF, Becker C, Johnson TR. Cervical and cranial computed tomographic angiography with automated bone removal: dual energy computed tomography versus standard computed tomography. Invest Radiol 2009; 44:293–297.
36. Hegde A, Chan LL, Tan L, Illyyas M, Lim WE. Dual Energy CT and its use in neuroangiography. Ann Acad Med Singapore 2009; 38:817–820.
37. Gorgos A, Remy-Jardin M, Duhamel A, et al. Evaluation of peripheral pulmonary arteries at 80 kV and at 140 kV: dual-energy computed tomography assessment in 51 patients. J Comput Assist Tomogr 2009; 33:981–986.
38. Lee CW, Seo JB, Song JW, et al. Evaluation of computer-aided detection and dual energy software in detection of peripheral pulmonary embolism on dual-energy pulmonary CT angiography. Eur Radiol 2011; 21:54–62.
39. Lu GM, Wu SY, Yeh BM, Zhang LJ. Dual-energy computed tomography in pulmonary embolism. Br J Radiol 2010; 83:707–718.
40. Krissak R, Henzler T, Reichert M, Krauss B, Schoenberg SO, Fink C. Enhanced visualization of lung vessels for diagnosis of pulmonary embolism using dual energy CT angiography. Invest Radiol 2010; 45:341–346.
41. Chae EJ, Seo JB, Jang YM, et al. Dual-energy CT for assessment of the severity of acute pulmonary embolism: pulmonary perfusion defect score compared with CT angiographic obstruction score and right ventricular/left ventricular diameter ratio. AJR Am J Roentgenol 2010; 194:604–610.
42. Fink C, Johnson TR, Michaely HJ, et al. Dual-energy CT angiography of the lung in patients with suspected pulmonary embolism: initial results. Rofo 2008; 180:879–883.
43. Pontana F, Faivre JB, Remy-Jardin M, et al. Lung perfusion with dual-energy multidetector-row CT (MDCT): feasibility for the evaluation of acute pulmonary embolism in 117 consecutive patients. Acad Radiol 2008; 15:1494–1504.
44. Renard B, Remy-Jardin M, Santangelo T, et al. Dual-energy CT angiography of chronic thromboembolic disease: can it help recognize links between the severity of pulmonary arterial obstruction and perfusion defects? Eur J Radiol 2010 May 18. [Epub ahead of print] doi:10.1016/j.ejrad.2010.04.018.
45. Goo HW. Initial experience of dual-energy lung perfusion CT using a dual-source CT system in children. Pediatr Radiol 2010; 40:1536–1544.

46. Pontana F, Remy-Jardin M, Duhamel A, Faivre JB, Wallaert B, Remy J. Lung perfusion with dual-energy multi-detector row CT: can it help recognize ground glass opacities of vascular origin? Acad Radiol 2010; 17:587–594.
47. Thieme SF, Johnson TR, Lee C, et al. Dual-energy CT for the assessment of contrast material distribution in the pulmonary parenchyma. AJR Am J Roentgenol 2009; 193:144–149.
48. Thieme SF, Becker CR, Hacker M, Nikolaou K, Reiser MF, Johnson TR. Dual energy CT for the assessment of lung perfusion--correlation to scintigraphy. Eur J Radiol 2008; 68:369–374.
49. Kang MJ, Park CM, Lee CH, Goo JM, Lee HJ. Dual-energy CT: clinical applications in various pulmonary diseases. Radiographics 2010; 30:685–698.
50. Lacout A, Marcy PY, El Hajjam M. Assessment of lobar perfusion in smokers according to the presence and severity of emphysema: preliminary experience with dual-energy CT angiography. Eur Radiol 2010; 20:2588–2589.
51. Park EA, Goo JM, Park SJ, Lee HJ, et al. Chronic obstructive pulmonary disease: quantitative and visual ventilation pattern analysis at xenon ventilation CT performed by using a dual-energy technique. Radiology 2010; 256:985–997.
52. Thieme SF, Hoegl S, Nikolaou K, et al. Pulmonary ventilation and perfusion imaging with dual-energy CT. Eur Radiol 2010; 20:2882–2889.
53. Chae EJ, Seo JB, Lee J, et al. Xenon ventilation imaging using dual-energy computed tomography in asthmatics: initial experience. Invest Radiol 2010; 45:354–361.
54. Chae EJ, Seo JB, Goo HW, et al. Xenon ventilation CT with a dual-energy technique of dual-source CT: initial experience. Radiology 2008; 248:615–624.
55. Ferda J, Ferdová E, Mírka H, et al. Pulmonary imaging using dual-energy CT, a role of the assessment of iodine and air distribution. Eur J Radiol 2009 Aug 28. [Epub ahead of print] doi:10.1016/j.ejrad.2009.08.005.
56. Goodsitt MM, Chan HP, Way TW, Schipper MJ, Larson SC, Christodoulou EG. Quantitative CT of lung nodules: dependence of calibration on patient body size, anatomic region, and calibration nodule size for single- and dual-energy techniques. Med Phys 2009; 36:3107–3121.
57. Chae EJ, Song JW, Seo JB, Krauss B, Jang YM, Song KS. Clinical utility of dual-energy CT in the evaluation of solitary pulmonary nodules: initial experience. Radiology 2008; 249:671–681.
58. Remy-Jardin M, Faivre JB, Pontana F, et al. Thoracic applications of dual energy. Radiol Clin North Am 2010; 48:193–205.
59. Kang DK, Schoepf UJ, Bastarrika G, et al. Dual-energy computed tomography for integrative imaging of coronary artery disease: principles and clinical applications. Semin Ultrasound CT MR 2010; 31:276–291.
60. Ruzsics B, Lee H, Zwerner PL, Gebregziabher M, Costello P, Schoepf UJ. Dual-energy CT of the heart for diagnosing coronary artery stenosis and myocardial ischemia-initial experience. Eur Radiol 2008; 18:2414–2424.
61. Ruzsics B, Schwarz F, Schoepf UJ, et al. Comparison of dual-energy computed tomography of the heart with single photon emission computed tomography for assessment of coronary artery stenosis and of the myocardial blood supply. Am J Cardiol 2009; 104:318–326.
62. Ko SM, Choi JW, Song MG, et al. Myocardial perfusion imaging using adenosine-induced stress dual-energy computed tomography of the heart: comparison with cardiac magnetic resonance imaging and conventional coronary angiography. Eur Radiol 2011; 21:26–35.
63. Nagao M, Kido T, Watanabe K, et al. Functional assessment of coronary artery flow using adenosine stress dual-energy CT: a preliminary study. Int J Cardiovasc Imaging 2011; 27:471–481.
64. Schwarz F, Ruzsics B, Schoepf UJ, et al. Dual-energy CT of the heart-principles and protocols. Eur J Radiol 2008; 68:423–433.
65. Bauer RW, Kerl JM, Fischer N, et al. Dual-energy CT for the assessment of chronic myocardial infarction in patients with chronic coronary artery disease: comparison with 3-T MRI. AJR Am J Roentgenol 2010; 195:639–646.
66. Zhang LJ, Peng J, Wu SY, Yeh BM, Zhou CS, Lu GM. Dual source dual-energy computed tomography of acute myocardial infarction: correlation with histopathologic findings in a canine model. Invest Radiol 2010; 45:290–297.
67. Hazirolan T, Akpinar B, Unal S, Gümrük F, Haliloglu M, Alibek S. Value of dual energy computed tomography for detection of myocardial iron deposition in thalassaemia patients: initial experience. Eur J Radiol 2008; 68:442–445.
68. Tanami Y, Ikeda E, Jinzaki M, et al. Computed tomographic attenuation value of coronary atherosclerotic plaques with different tube voltage: an ex vivo study. J Comput Assist Tomogr 2010; 34:58–63.
69. Halpern EJ, Halpern DJ, Yanof JH, et al. Is coronary stent assessment improved with spectral analysis of dual energy CT? Acad Radiol 2009; 16:1241–1250.
70. Barreto M, Schoenhagen P, Nair A, et al. Potential of dual-energy computed tomography to characterize atherosclerotic plaque: ex vivo assessment of human coronary arteries in comparison to histology. J Cardiovasc Comput Tomogr 2008; 2:234–242.
71. Boll DT, Merkle EM, Paulson EK, Mirza RA, Fleiter TR. Calcified vascular plaque specimens: assessment with cardiac dual-energy multidetector CT in anthropomorphically moving heart phantom. Radiology 2008; 249:119–126.
72. Boll DT, Merkle EM, Paulson EK, Fleiter TR. Coronary stent patency: dual-energy multidetector CT assessment in a pilot study with anthropomorphic phantom. Radiology 2008; 247:687–95.
73. Chandarana H, Godoy MC, Vlahos I, et al. Abdominal aorta: evaluation with dual-source dual-energy multidetector CT after endovascular repair of aneurysms--initial observations. Radiology 2008; 249:692–700.
74. Numburi UD, Schoenhagen P, Flamm SD, et al. Feasibility of dual-energy CT in the arterial phase: Imaging after endovascular aortic repair. AJR Am J Roentgenol 2010; 195:486–493.
75. Sommer WH, Graser A, Becker CR, et al. Image quality of virtual noncontrast images derived from dual-energy CT angiography after endovascular aneurysm repair. J Vasc Interv Radiol 2010; 21:315–321.
76. Stolzmann P, Frauenfelder T, Pfammatter T, et al. Endoleaks after endovascular abdominal aortic aneurysm repair: detection with dual-energy dual-source CT. Radiology 2008; 249:682–691.
77. Laks S, Macari M, Chandarana H. Dual-energy computed tomography imaging of the aorta after endovascular repair of abdominal aortic aneurysm. Semin Ultrasound CT MR 2010; 31:292–300.
78. Behrendt FF, Schmidt B, Plumhans C, et al. Image fusion in dual energy computed tomography: effect on contrast enhancement, signal-to-noise ratio and image quality in computed tomography angiography. Invest Radiol 2009; 44:1–6.
79. Brockmann C, Jochum S, Sadick M, et al. Dual-energy CT angiography in peripheral arterial occlusive disease. Cardiovasc Intervent Radiol 2009; 32:630–637.
80. Tran DN, Straka M, Roos JE, Napel S, Fleischmann D. Dual-energy CT discrimination of iodine and calcium: experimental results and implications for lower extremity CT angiography. Acad Radiol 2009; 16:160–171.
81. Meyer BC, Werncke T, Hopfenmüller W, Raatschen HJ, Wolf KJ, Albrecht T. Dual energy CT of peripheral arteries: effect of automatic bone and plaque removal on image quality and grading of stenoses. Eur J Radiol 2008; 68:414–422.
82. Werncke T, Albrecht T, Wolf KJ, Meyer BC. [Dual energy CT of the peripheral arteries: a phantom study to assess the effect of automatic plaque removal on stenosis grading] Rofo 2010; 182:682–689.
83. Sommer WH, Johnson TR, Becker CR, et al. The value of dual-energy bone removal in maximum intensity projections of lower extremity computed tomography angiography. Invest Radiol 2009; 44:285–292.
84. Yamamoto S, McWilliams J, Arellano C, et al. Dual-energy CT angiography of pelvic and lower extremity arteries: dual-energy bone subtraction versus manual bone subtraction. Clin Radiol 2009; 64:1088–1096.
85. Zachrisson H, Engström E, Engvall J, Wigström L, Smedby O, Persson A. Soft tissue discrimination ex vivo by dual energy computed tomography. Eur J Radiol 2010; 75:e124–28.
86. Yeh BM, Shepherd JA, Wang ZJ, Teh HS, Hartman RP, Prevrhal S. Dual-energy and low-kVp CT in the abdomen. AJR Am J Roentgenol 2009; 193:47–54.
87. Graser A, Johnson TR, Chandarana H, Macari M. Dual energy CT: preliminary observations and potential clinical applications in the abdomen. Eur Radiol 2009; 19:13–23.
88. Coursey CA, Nelson RC, Boll DT, et al. Dual-energy multidetector CT: how does it work, what can it tell us, and when can we use it in abdominopelvic imaging? Radiographics 2010; 30:1037–1055.

89. Robinson E, Babb J, Chandarana H, Macari M. Dual source dual energy MDCT: comparison of 80 kVp and weighted average 120 kVp data for conspicuity of hypo-vascular liver metastases. Invest Radiol 2010; 45:413–418.
90. Marin D, Nelson RC, Schindera ST, et al. Low-tube-voltage, high-tube-current multidetector abdominal CT: improved image quality and decreased radiation dose with adaptive statistical iterative reconstruction algorithm--initial clinical experience. Radiology 2010; 254:145–153.
91. Kim KS, Lee JM, Kim SH, et al. Image fusion in dual energy computed tomography for detection of hypervascular liver hepatocellular carcinoma: phantom and preliminary studies. Invest Radiol 2010; 45:149–157.
92. Zhang LJ, Peng J, Wu SY, et al. Liver virtual non-enhanced CT with dual-source, dual-energy CT: a preliminary study. Eur Radiol 2010; 20:2257–2264.
93. De Cecco CN, Buffa V, Fedeli S, et al. Dual energy CT (DECT) of the liver: conventional versus virtual unenhanced images. Eur Radiol 2010; 20:2870-2875.
94. Raptopoulos V, Karellas A, Bernstein J, Reale FR, Constantinou C, Zawacki JK. Value of dual-energy CT in differentiating focal fatty infiltration of the liver from low-density masses. AJR Am J Roentgenol 1991; 157:721–725.
95. Sommer CM, Schwarzwaelder CB, Stiller W, et al. Dual-energy computed-tomography cholangiography in potential donors for living-related liver transplantation: initial experience. Invest Radiol 2010; 45:406–412.
96. Bauer RW, Schulz JR, Zedler B, Graf TG, Vogl TJ. Compound analysis of gallstones using dual energy computed tomography--results in a phantom model. Eur J Radiol 2010; 75:e74–80.
97. Voit H, Krauss B, Heinrich MC, et al. [Dual-source CT: in vitro characterization of gallstones using dual energy analysis] Rofo 2009; 181:367–373.
98. Marin D, Nelson RC, Barnhart H, et al. Detection of pancreatic tumors, image quality, and radiation dose during the pancreatic parenchymal phase: effect of a low-tube-voltage, high-tube-current CT technique--preliminary results. Radiology 2010; 256:450–459.
99. Macari M, Spieler B, Kim D, et al. Dual-source dual-energy MDCT of pancreatic adenocarcinoma: initial observations with data generated at 80 kVp and at simulated weighted-average 120 kVp. AJR Am J Roentgenol 2010; 194:W27–32.
100. Karcaaltincaba M, Karaosmanoglu D, Akata D, Sentürk S, Ozmen M, Alibek S. Dual energy virtual CT colonoscopy with dual source computed tomography: initial experience. Rofo 2009; 181:859–862.
101. Eliahou R, Azraq Y, Carmi R, Mahgerefteh SY, Sosna J. Dual-energy based spectral electronic cleansing in non-cathartic computed tomography colonography: an emerging novel technique. Semin Ultrasound CT MR 2010; 31:309–314.
102. Vrtiska TJ, Takahashi N, Fletcher JG, Hartman RP, Yu L, Kawashima A. Genitourinary applications of dual-energy CT. AJR Am J Roentgenol 2010; 194:1434–1442.
103. Primak AN, Fletcher JG, Vrtiska TJ, et al. Noninvasive differentiation of uric acid versus non-uric acid kidney stones using dual-energy CT. Acad Radiol 2007; 14: 1441–1447.
104. Scheffel H, Stolzmann P, Frauenfelder T, et al. Dual-energy contrast-enhanced computed tomography for the detection of urinary stone disease. Invest Radiol 2007; 42:823–829.
105. Graser A, Johnson TR, Bader M, et al. Dual energy CT characterization of urinary calculi: initial in vitro and clinical experience. Invest Radiol 2008; 43:112–119.
106. Grosjean R, Sauer B, Guerra RM e al. Characterization of human renal stones with MDCT: advantage of dual energy and limitations due to respiratory motion. AJR Am J Roentgenol 2008; 190:720–728.
107. Stolzmann P, Kozomara M, Chuck N, et al. In vivo identification of uric acid stones with dual-energy CT: diagnostic performance evaluation in patients. Abdom Imaging 2010; 35:629–635.
108. Thomas C, Patschan O, Ketelsen D, et al. Dual-energy CT for the characterization of urinary calculi: in vitro and in vivo evaluation of a low-dose scanning protocol. Eur Radiol 2009; 19:1553–1559.
109. Boll DT, Patil NA, Paulson EK, et al. Renal stone assessment with dual-energy multidetector CT and advanced postprocessing techniques: improved characterization of renal stone composition--pilot study. Radiology 2009; 250:813–820.
110. Stolzmann P, Leschka S, Scheffel H, et al. Characterization of urinary stones with dual-energy CT: improved differentiation using a tin filter. Invest Radiol 2010; 45:1–6.
111. Thomas C, Krauss B, Ketelsen D, et al. Differentiation of urinary calculi with dual energy CT: effect of spectral shaping by high energy tin filtration. Invest Radiol 2010; 45:393–398.
112. Takahashi N, Hartman RP, Vrtiska TJ, et al. Dual-energy CT iodine-subtraction virtual unenhanced technique to detect urinary stones in an iodine-filled collecting system: a phantom study. AJR Am J Roentgenol 2008; 190:1169–1173.
113. Takahashi N, Vrtiska TJ, Kawashima A, et al. Detectability of urinary stones on virtual nonenhanced images generated at pyelographic-phase dual-energy CT. Radiology 2010; 256:184–190.
114. Graser A, Johnson TR, Hecht EM, et al. Dual-energy CT in patients suspected of having renal masses: can virtual nonenhanced images replace true nonenhanced images? Radiology 2009; 252:433–440.
115. Graser A, Becker CR, Staehler M, et al. Single-phase dual-energy CT allows for characterization of renal masses as benign or malignant. Invest Radiol 2010; 45:399–405.
116. Leschka S, Stolzmann P, Baumüller S, et al. Performance of dual-energy CT with tin filter technology for the discrimination of renal cysts and enhancing masses. Acad Radiol 2010; 17:526–534.
117. Brown CL, Hartman RP, Dzyubak OP, et al. Dual-energy CT iodine overlay technique for characterization of renal masses as cyst or solid: a phantom feasibility study. Eur Radiol 2009; 19:1289–1295.
118. Karlo C, Lauber A, Götti RP, et al. Dual-energy CT with tin filter technology for the discrimination of renal lesion proxies containing blood, protein, and contrast-agent. An experimental phantom study. Eur Radiol 2011; 21:385–392.
119. Gupta RT, Ho LM, Marin D, et al. Dual-energy CT for characterization of adrenal nodules: initial experience. AJR Am J Roentgenol 2010; 194:1479–1483.
120. Nicolaou S, Yong-Hing CJ, Galea-Soler S, Hou DJ, Louis L, Munk P. Dual-energy CT as a potential new diagnostic tool in the management of gout in the acute setting. AJR Am J Roentgenol 2010; 194:1072–1078.
121. Artmann A, Ratzenböck M, Noszian I, Trieb K. [Dual energy CT--a new perspective in the diagnosis of gout] Rofo 2010; 182:261–266.
122. Choi HK, Al-Arfaj AM, Eftekhari A, et al. Dual energy computed tomography in tophaceous gout. Ann Rheum Dis 2009; 68:1609–1612.
123. Deng K, Sun C, Liu C, Ma R. Initial experience with visualizing hand and foot tendons by dual-energy computed tomography. Clin Imaging 2009; 33:384–389.
124. Lohan DG, Motamedi K, Chow K, et al. Does dual-energy CT of lower-extremity tendons incur penalties in patient radiation exposure or reduced multiplanar reconstruction image quality? AJR Am J Roentgenol 2008; 191:1386–1390.
125. Sun C, Miao F, Wang XM, et al. An initial qualitative study of dual-energy CT in the knee ligaments. Surg Radiol Anat 2008; 30:443–447.
126. Subhas N, Freire M, Primak AN, et al. CT arthrography: in vitro evaluation of single and dual energy for optimization of technique. Skeletal Radiol 2010; 39:1025–1031.
127. Pache G, Krauss B, Strohm P, et al. Dual-energy CT virtual noncalcium technique: detecting posttraumatic bone marrow lesions--feasibility study. Radiology 2010; 256:617–624.
128. Sangwaiya MJ, Kalra MK, Sharma A, Halpern EF, Shepard JA, Digumarthy SR. Dual-energy computed tomographic pulmonary angiography: a pilot study to assess the effect on image quality and diagnostic confidence. J Comput Assist Tomogr 2010; 34:46–51.
129. Hoey ET, Gopalan D, Ganesh V, Agrawal SK, Qureshi N, Tasker AD, Clements L, Screaton NJ. Dual-energy CT pulmonary angiography: a novel technique for assessing acute and chronic pulmonary thromboembolism. Clin Radiol 2009; 64: 414–419.